

Microstructure, Texture, and Hardness Evolution of Cold-Rolled High-Purity Ti Sheet During Annealing at 350 °C to 550 °C



XING HU, LINJIANG CHAI, JING SHEN, HAO WU, YUQIONG LI, JUN CHENG, JINRU LUO, and LEI YAO

The microstructural, textural, and hardness evolution of a cold-rolled high-purity Ti sheet (50 pct reduction in thickness) during isochronal annealing at 350 °C to 550 °C was investigated by jointly using electron backscatter diffraction, electron channel contrast imaging, X-ray diffraction, and hardness test, with a dedicated correlation analysis between them performed. Results show that recrystallization nucleation starts at 400 °C with prior grain boundaries as preferential sites while fully recrystallized structures were obtained after annealing at 550 °C for 1 hours. During the primary recrystallization, contrary to earlier reports, considerable textural changes occur: the prior bimodal basal texture characteristic is essentially replaced by a ring-like basal texture. Such a textural change is attributed to the orientation-gradient-related subgrain coalescence mechanism that dominates the recrystallization nucleation of the high-purity Ti sheet. Specimen hardness always decreases with increasing the annealing temperature (from 234.3 ± 5.8 to 135.9 ± 2.9 HV), which is closely related to continuous variations of grain sizes and dislocation densities (mainly stored in low-angle boundaries). Quantitative analyses reveal that both grain sizes and dislocation densities have mild effects on the hardness change when annealed below 450 °C. However, the decrease in dislocation density leads to more significant softening than grain coarsening when the annealing temperature exceeds 450 °C.

<https://doi.org/10.1007/s11661-022-06651-z>

© The Minerals, Metals & Materials Society and ASM International 2022

I. INTRODUCTION

TITANIUM (Ti) and its alloys are widely used in aerospace, chemical, and biomedical fields due to its excellent properties like high specific strength, good corrosion resistance, and bio-compatibility.^[1–3] At room temperature, pure Ti and low alloyed Ti alloys mainly consist of α phase with a hexagonal close packed (HCP)

structure. Compared to cubic metals, fewer slip systems are operable in α -Ti and twinning frequently occurs, leading its plastic deformation mechanisms to be relatively complicated.^[4–6] Among all kinds of Ti-based materials, sheets/plates processed by rolling and subsequent heat treatments are the most important ones because of their overwhelmingly large consumption. For the sheets/plates with α -Ti as the major constituent phase, their specific deformation behaviors often allow numerous twins and strong crystallographic textures to be induced during rolling.^[7,8] Once subjected to annealing, such features would markedly affect grain boundary migration, recrystallization nucleation, and grain growth behaviors. To date, microstructural and textural evolution of rolled α -Ti sheets during annealing has been tentatively explored.^[9–13] Hayama *et al.*^[9] reported that for a coarse-grained pure Ti sheet after 50 pct rolling, recrystallized structures fully comprised of equiaxed grains could be obtained after annealing at 700 °C for 15 minutes. Ghosh *et al.*^[11] performed unidirectional and multi-step cross rolling (upto 90 pct reduction in thickness) for a commercially pure Ti (CP-Ti) sheet and found that the non-oriented nucleation was more likely to occur in the former one during recrystallization annealing. Through systematic studies, Sahoo *et al.*^[12]

XING HU, LINJIANG CHAI, JING SHEN, and HAO WU are with the College of Materials Science and Engineering, Chongqing University of Technology, Chongqing 400054, China. Contact e-mail: chailinjiang@cqut.edu.cn YUQIONG LI is with the MOE Key Laboratory of New Processing Technology for Non-ferrous Metals and Materials, Guangxi Key Laboratory of Processing for Non-ferrous Metals and Featured Materials, Guangxi University, Nanning 530004, China. JUN CHENG is with the Shaanxi Key Laboratory of Biomedical Metal Materials, Northwest Institute for Nonferrous Metal Research, Xi'an 710016, China. JINRU LUO is with the Institute of Material, China Academy of Engineering Physics, Mianyang 621908, China. Contact e-mail: ada669@qq.com LEI YAO is with the School of Nuclear Science and Technology, University of South China, Hengyang 421001, China and also with the Hunan Engineering & Technology Research Center for Virtual Nuclear Reactor, University of South China, Hengyang 421001, China. Contact e-mail: 1875318348@qq.com

Manuscript submitted November 11, 2021; accepted March 6, 2022.

Article published online March 25, 2022

noted that the texture of a heavily rolled CP-Ti sheet would hardly be changed after primary recrystallization.

Note that most pure Ti sheets used for revealing recrystallization behaviors in earlier work have the “commercial purity.” In fact, the presence of specific impurities or alloying elements in CP-Ti may have a significant impact on its deformation microstructure and texture,^[14–16] and further affect recrystallization nucleation and grain growth during annealing.^[17,18] Thus, compared to those already reported for CP-Ti, distinct microstructural and textural characteristics could be anticipated for high-purity Ti (HP-Ti) during rolling and annealing. Dedicated studies of effects of annealing temperatures on microstructural and textural evolution of rolled HP-Ti sheets should be helpful for more comprehensively and accurately understanding the recrystallization mechanism of α -Ti.

In the present study, therefore, a cold-rolled HP-Ti sheet (50 pct reduction in thickness) was subjected to isochronal annealing at 350 °C to 550 °C for 1 hours, with microstructural and textural characteristics revealed by jointly using electron backscatter diffraction (EBSD), electron channel contrast (ECC) imaging, and X-ray diffraction (XRD) techniques. Afterward, hardness was measured for both rolled and annealed specimens and a quantitative correlation analysis was then made between microstructural, textural characteristics and hardness.

II. EXPERIMENTAL MATERIALS AND METHODS

The starting material was a HP-Ti sheet (1.3 mm in thickness; 99.99 wt pct in purity) after 50 pct rolling in thickness reduction at room temperature. Rectangular specimens with dimensions of 8 mm (RD) \times 6 mm (TD) \times 1.3 mm (ND) were cut from the starting sheet, with RD, TD, and ND corresponding to rolling, transverse, and normal directions of the sheet, respectively. The as-cut specimens were sealed into quartz tubes under vacuum ($\leq 10^{-3}$ Pa) and then annealed in a programmable box furnace at 350 °C, 400 °C, 450 °C, 500 °C, and 550 °C for 1 hours, respectively, followed immediately by water quenching.

Microstructural and textural characteristics of various specimens were mainly characterized by EBSD and ECC imaging techniques in a field emission gun scanning electron microscope (Zeiss Sigma HD). The EBSD system consisted of a NordlysMax² detector (Oxford Instruments) with Aztec 3.1 and HKL Channel 5 software for data acquisition and post-processing, respectively. Note that the EBSD data specifically used for texture analyses were collected with relatively large scanning areas (0.8 mm²), so that a reasonable number of grain orientations could be included. Additionally, diffraction preferences of various specimens were examined by XRD (PANalytical Empyrean Series 2) with Cu K $_{\alpha}$ radiation. For hardness measurements, a Vickers indentation tester was employed, with 12 measurements (at a load of 100 g for 10 seconds) made for each specimen to calculate an average value. Before the above

characterizations and examinations, the to-be-examined planes (RD-ND plane for EBSD and ECC; RD-TD plane for XRD) of all specimens were mechanically ground by SiC papers and further electro-polished with a mixed solution of 10 pct perchloric acid and 90 pct methanol at 14 V and -30 °C for 120 seconds.

III. RESULTS

A. Microstructural Characteristics

ECC observations of the as-rolled specimen and specimens annealed at various temperatures are presented in Figures 1 and 2. From Figure 1(a), it is seen that the as-rolled HP-Ti sheet has no clear grain morphologies while dense twinning lamellae can be observed at high-magnification observation (Figure 2(a)), indicating heavy plastic deformation induced by the 50 pct rolling. Figure 1(b) shows that microstructural characteristics of the specimen annealed at 350 °C for 1 hours are essentially the same as that of the as-rolled specimen. After increasing the annealing temperature to 400 °C, a few small crystallites appear with distinct contrasts from surrounding deformed structures (Figure 1(c)). A closer observation (Figure 2(b)) reveals that they are recrystallization nuclei (a few micrometers in size) without internal distortions/defects, in strong contrast with surrounding shear bands, twins, or dislocation cells, clearly indicating the occurrence of recrystallization behavior. As the temperature increases to 450 °C (Figures 1(d) and 2(c)), the number and size of the recrystallization nuclei increase significantly. Figure 1(e) presents the microstructure of the 500 °C-annealed specimen, from which one can see that most of the prior deformed structures have been replaced by recrystallized structures. Even for those unrecrystallized lamellae, Figure 2(d) suggests higher contrast differences existing between them, which may be related to gradual reorientation through dislocation rearrangement by recovery. After annealing at 550 °C for 1 hours, fully recrystallized structures with well-recrystallized grains are developed and no residual deformed structures can be found, indicating the completion of primary recrystallization.

Figure 3 presents EBSD band contrast (BC) maps of the as-rolled and the annealed specimens. The relatively low image quality in Figure 3(a) suggests the presence of numerous deformation defects in the as-rolled specimen. After annealing at 350 °C for 1 hours, the image quality seems to be slightly improved but no recrystallization nuclei can be clearly defined (Figure 3(b)). Such change might be mainly related to release of a part of stored energy by recovery, which often plays the role of a precursor for the recrystallization nucleation.^[19] After the annealing temperature reaches 400 °C, a few recrystallization nuclei can be easily distinguished from the deformed structures (Figure 3(c)). The much brighter contrast of these nuclei indicates the absence of considerable internal defects. With further raising the annealing temperature to 450 °C and 500 °C, the

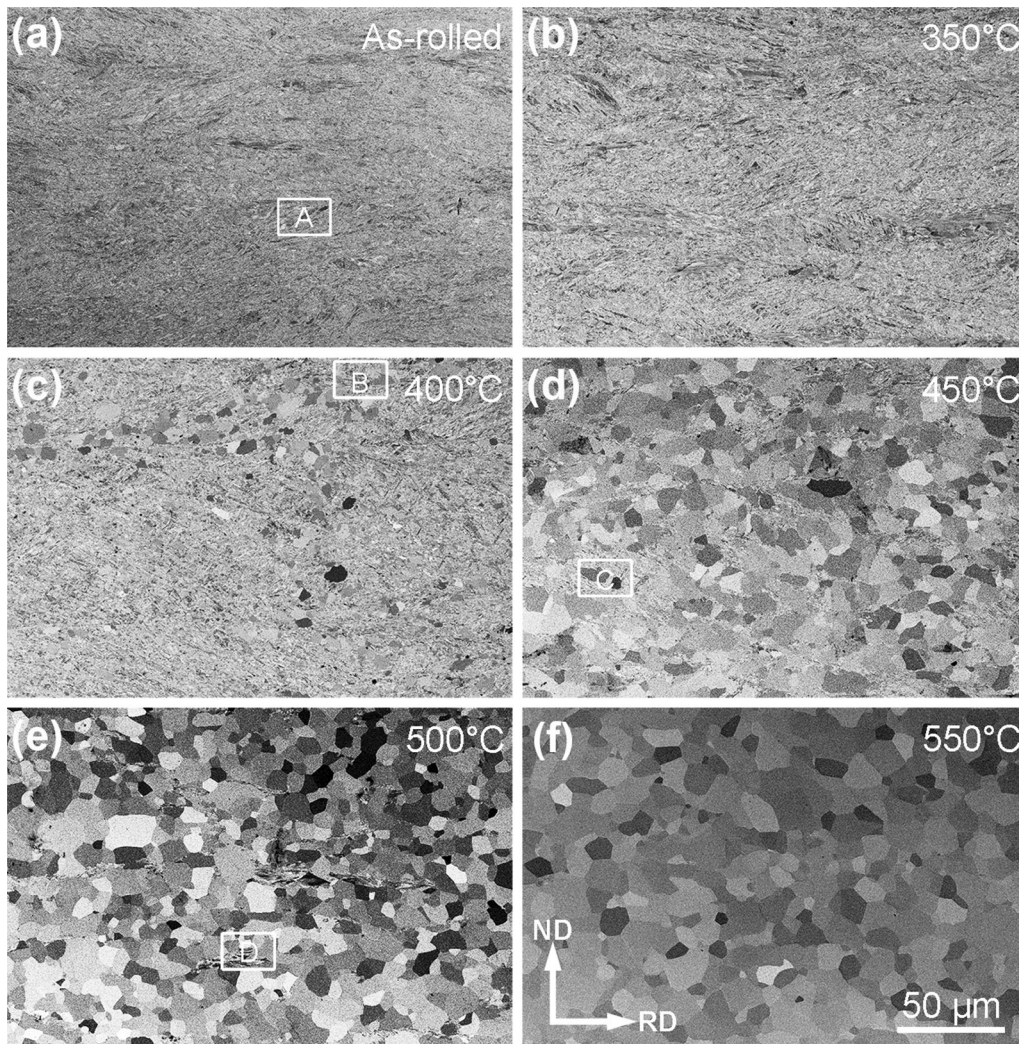


Fig. 1—ECC images of the (a) as-rolled HP-Ti sheet and specimens annealed at various temperatures: (b) 350 °C, (c) 400 °C, (d) 450 °C, (e) 500 °C, and (f) 550 °C, respectively.

fraction of the recrystallized structures continues to increase at the expense of the deformed structures. After annealing at 550 °C for 1 hours, a rather uniform microstructure consisting of well-recrystallized grains is obtained with the absence of all deformed structures, clearly indicating the primary recrystallization to be completed, in good agreement with the ECC observation in Figure 1(f).

Figure 4 shows inverse pole figure (IPF) maps corresponding to Figure 3, with low-angle boundaries (LABs, $2 \text{ deg} < \theta < 15 \text{ deg}$) and high-angle boundaries (HABs, $\theta > 15 \text{ deg}$) delineated by silver and black lines, respectively. It is seen from Figure 4(a), there exist both small crystallites and lamellar structures enclosed by HABs in the as-rolled HP-Ti sheet, which should be resulted from sufficient twinning during rolling.^[8] By using the equivalent circle method,^[20] their average grain size is determined to be $1.9 \pm 1.4 \mu\text{m}$. Meanwhile, a large number of LABs can also be observed in Figure 4(a), suggesting dislocation slip to be activated by the prior rolling as well. After annealing at 350 °C (Figure 4(b)), compared to that in Figure 4(a), the grain

morphology is almost unchanged with an average grain size of $2.0 \pm 1.5 \mu\text{m}$. As the annealing temperature increases to 400 °C, a few new grains (recrystallization nuclei) without inside defects/substructures can be seen in Figure 4(c). Such defect-free grains seem to have different colors from the surrounding deformed structures, suggesting that the crystallographic texture (grain orientations) may have changed to some extent during the recrystallization. The average grain size of the 400 °C-annealed specimen is measured as $2.1 \pm 1.5 \mu\text{m}$. After further raising the annealing temperature to 450 °C and 500 °C, more recrystallized structures are developed (Figures 4(d) and (e)) with their average grain sizes increasing to 2.5 ± 2.3 and $3.7 \pm 3.6 \mu\text{m}$, respectively. When the as-rolled HP-Ti sheet is annealed at 550 °C for 1 hours, fully recrystallized structures are obtained with the average grain size measured to be $7.2 \pm 4.8 \mu\text{m}$. Most of these recrystallization grains are separated by HABs with hardly any LABs left.

Misorientation angle and rotation axis distributions of various specimens are presented in Figure 5. Figure 5(a) shows that the low-angle misorientation is

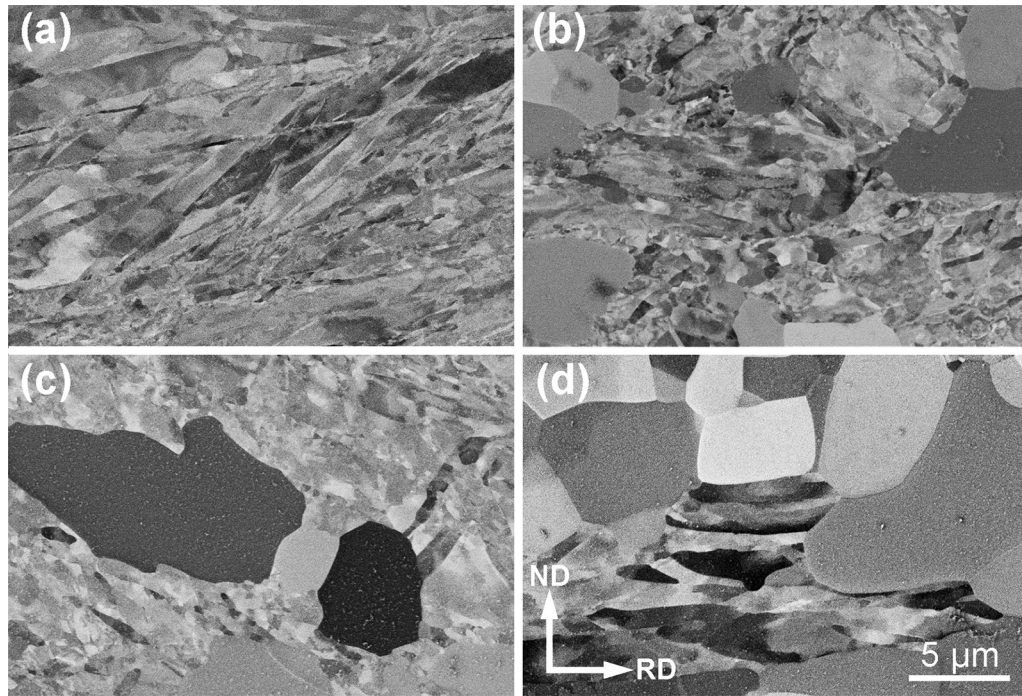


Fig. 2—(a to d) Magnified ECC observations corresponding to boxed regions A to D in Fig. 1.

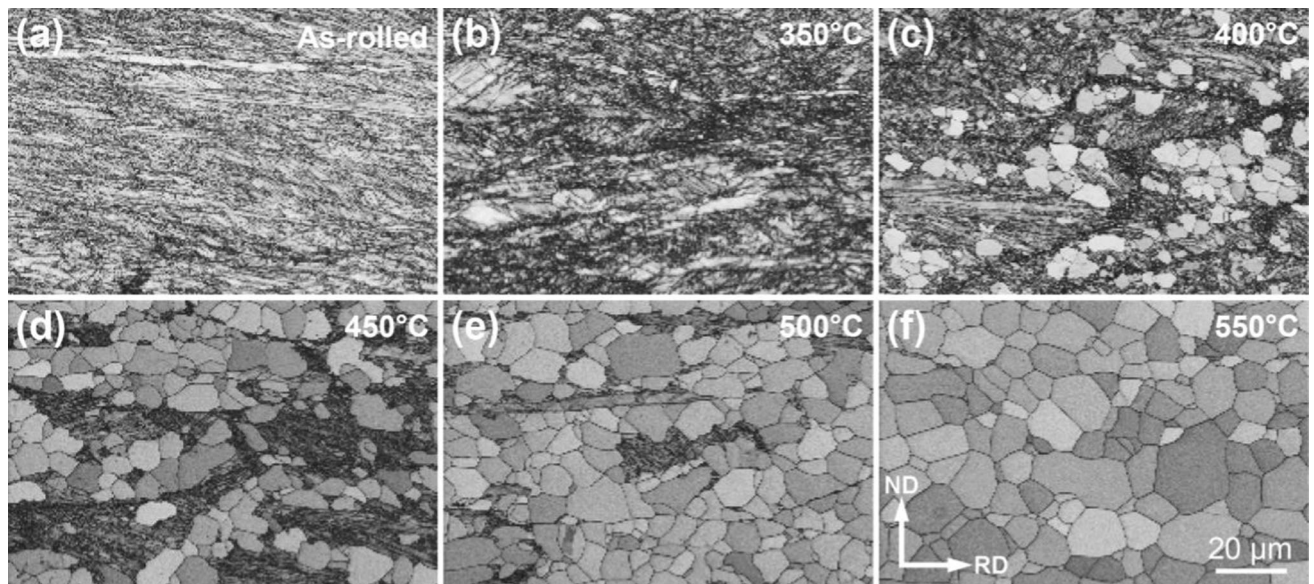


Fig. 3—EBSD BC maps (step size of $0.5 \mu\text{m}$) of the (a) as-rolled HP-Ti sheet and specimens annealed at various temperatures: (b) 350°C , (c) 400°C , (d) 450°C , (e) 500°C , and (f) 550°C , respectively.

predominant in the as-rolled specimen, along with two high-angle peaks near 65 and 85 deg. Their rotation axes are determined to be $\langle 10\bar{1}0 \rangle$ and $\langle 11\bar{2}0 \rangle$, respectively, coincident with angle/axis pairs of $\{10\bar{1}2\}\langle 10\bar{1}1 \rangle$ extension twinning and $\{11\bar{2}2\}\langle 11\bar{2}3 \rangle$ compression twinning boundaries.^[21,22] Such a misorientation characteristic is essentially unchanged after annealing at 350°C and 400°C (Figures 5(b) and (c)). When the annealing temperature increases to 450°C (Figure 5(d)), the LABs

content begins to drop. At higher temperatures, LABs are more effectively eliminated with HABs becoming overwhelmingly dominant in the 550°C -annealed specimen. It is revealed from Figures 1 through 4 that when the annealing temperature reaches 400°C the recrystallization nucleation begins to happen, the driving force of which comes from the deformation energy mainly stored in LABs.^[23,24] Initially, a few recrystallization nuclei can only produce a small number of HABs, leading the misorientation characteristic of the 400°C -annealed

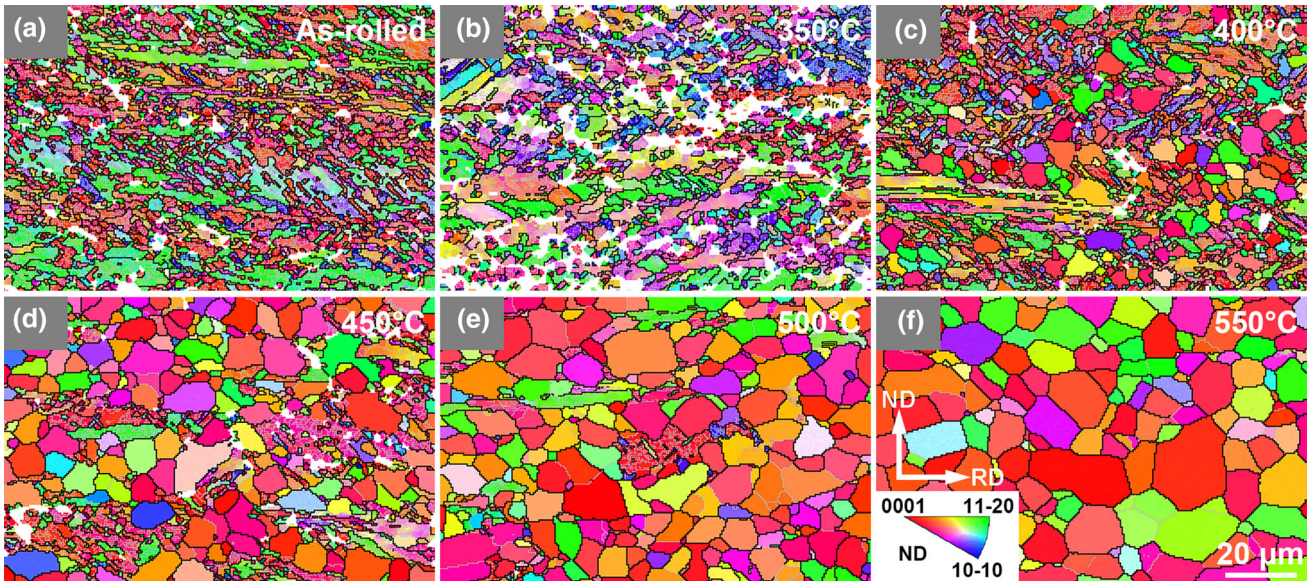


Fig. 4—EBSD IPF maps (corresponding to Fig. 3) of the (a) as-rolled HP-Ti sheet and specimens annealed at various temperatures: (b) 350 °C, (c) 400 °C, (d) 450 °C, (e) 500 °C, and (f) 550 °C, respectively.

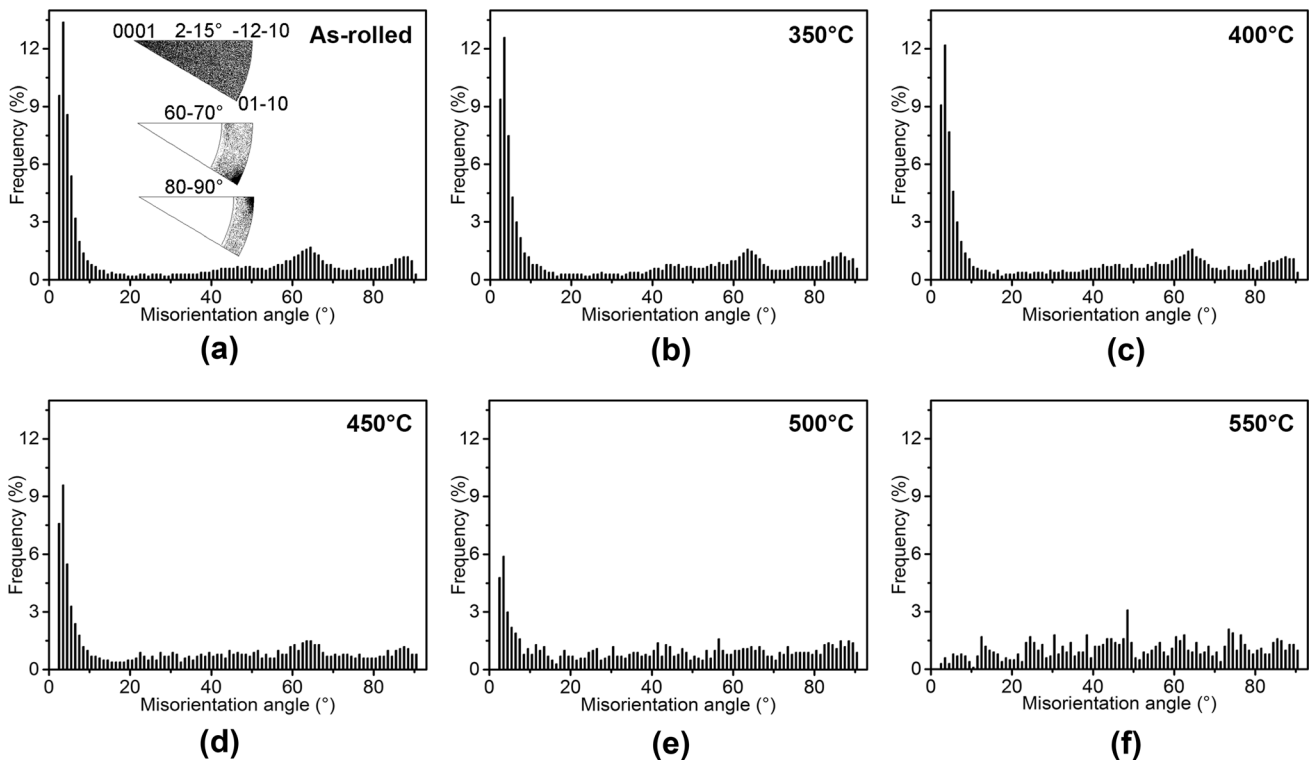


Fig. 5—Misorientation angle distributions (corresponding to Fig. 3) of the (a) as-rolled HP-Ti sheet and specimens annealed at various temperatures: (b) 350 °C, (c) 400 °C, (d) 450 °C, (e) 500 °C, and (f) 550 °C, respectively.

specimen (Figure 5(c)) to be still close to that of the as-rolled one (Figure 5(a)). After annealing at higher temperatures, more recrystallized structures are developed at the expense of deformed structures (including twinning lamellae). As a result, low-angle misorientations and those corresponding to twins are largely

reduced and replaced by common high-angle ones (common HABs) (Figures 5(d) through (f)).

Figures 6 and 7 are the kernel average misorientation (KAM) maps and distribution histograms of various specimens, respectively, which can be used to qualitatively reflect local strains and stored energy in metals.^[25] From Figures 6(a) and 7(a), the KAM distribution in

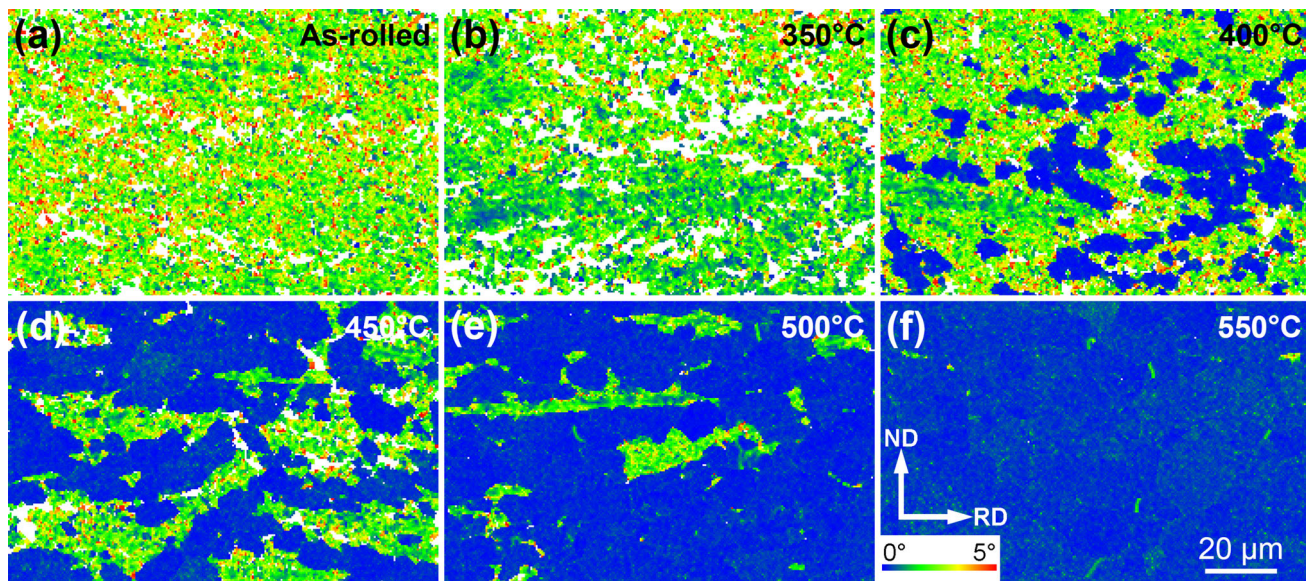


Fig. 6—EBSD KAM maps (corresponding to Fig. 3) of the (a) as-rolled HP-Ti sheet and specimens annealed at various temperatures: (b) 350 °C, (c) 400 °C, (d) 450 °C, (e) 500 °C, and (f) 550 °C, respectively (Color figure online).

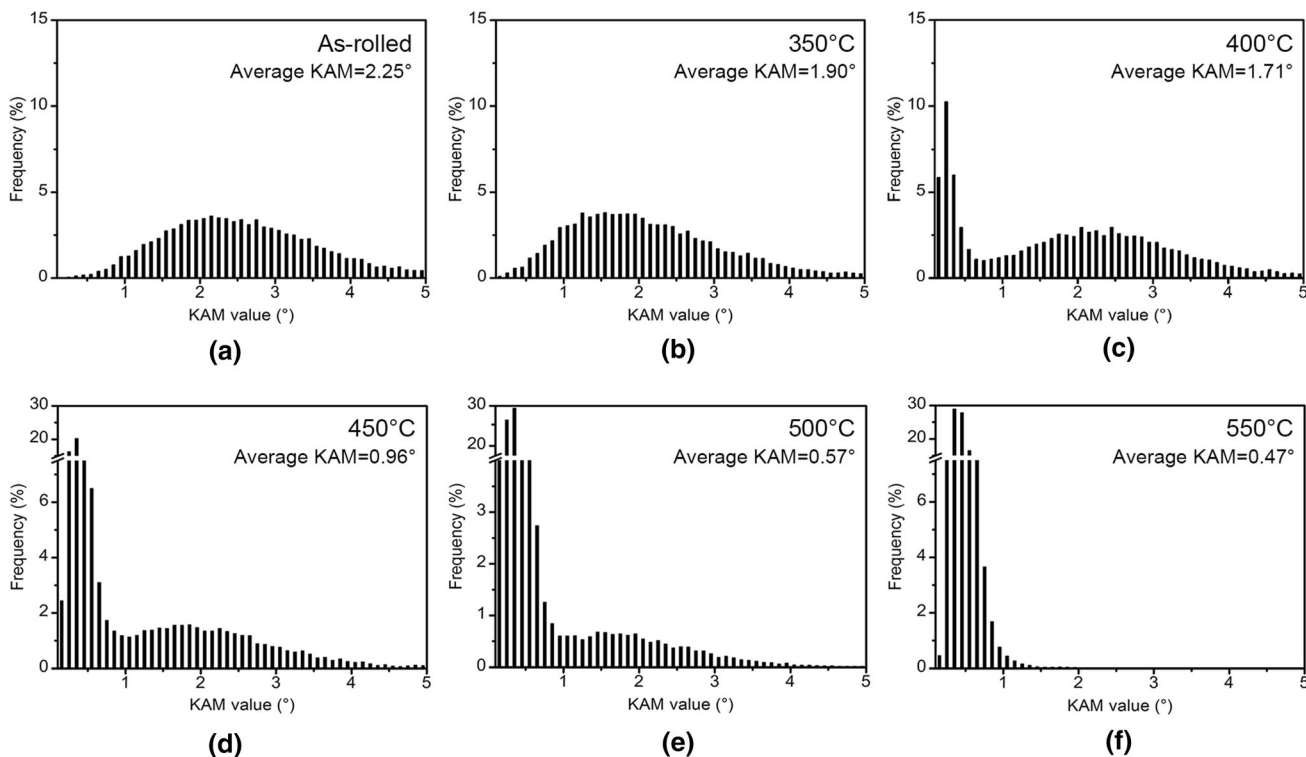


Fig. 7—KAM value distributions (corresponding to Fig. 3) of the (a) as-rolled HP-Ti sheet and specimens annealed at various temperatures: (b) 350 °C, (c) 400 °C, (d) 450 °C, (e) 500 °C, and (f) 550 °C, respectively.

the as-rolled specimen is generally uniform with a relatively high average KAM value (2.25 deg), indicating high local strains and stored energy induced by the prior rolling. With increasing the temperature from 350 °C to 500 °C, the average KAM value of the annealed specimens gradually decreases from 1.90 to 0.57 deg. In Figure 6(c) through (e), blue regions correspond to the

recrystallized structures in Figures 3 and 4, which have much lower KAM values than other regions (unrecrystallized). For the 550 °C-annealed specimen, Figure 6(f) shows that it is comprised of uniform blue structures with an average KAM value of only 0.47 deg. As indicated in Reference 25, such a low value demonstrates that almost no local strain or stored energy

remains present after the primary recrystallization is completed.

B. Textural Variation

Peak heights (intensities) in X-ray diffraction patterns reflect relative frequency of specific planes, which can be utilized to characterize the crystallographic texture qualitatively, as shown in Figure 8. For the as-rolled specimen, the diffraction intensities of (0002) and (10 $\bar{1}$ 1) planes are much higher than other crystal planes. After annealing at 350 °C, no evident change seems to occur. For the 400 °C-annealed specimen, diffraction intensities of both (0002) and (10 $\bar{1}$ 1) planes increase to a comparable height, along with slight intensifying of the (10 $\bar{1}$ 3) peak. Considering the appearance of recrystallization nuclei in this specimen, such variation suggests that a mild textural change may have occurred due to recrystallization nucleation. After annealing at higher temperatures, the diffraction intensity of the (10 $\bar{1}$ 1) plane increases rapidly to exceed that of the (0002) plane. The difference between the two planes becomes rather evident in the 550 °C-annealed specimen (fully recrystallized), suggesting that the recrystallization should have aroused considerable textural changes compared to that of the as-rolled specimen.

In order to more accurately analyze their textural features, a large-area EBSD scanning was performed for each specimen (thousands of grains included), with results presented in Figures 9 and 10. From pole figures (Figure 9(a)), the as-rolled HP-Ti sheet (50 pct reduction in thickness) has a typical bimodal basal texture with density maxima (5.0 times random) inclined $\pm\sim 30$ deg from the ND toward the TD, along with a weak c//TD component. After annealing at 350 °C (Figure 9(b)), since recrystallization nucleation is not initiated at all (Figure 3(b)), the textural characteristic is almost the same as that of the as-rolled specimen, consistent with that revealed in Figure 8. For the 400 °C-annealed specimen, although a few recrystallization nuclei appear (Figure 3(c)), the bimodal basal texture remains essentially unchanged, except further weakening of the c//TD component. After increasing the

annealing temperature to 450 °C, there appears a ring-like basal texture to replace the prior bimodal basal texture (Figure 9(d)). In a simplified description, the new textural characteristic may be roughly regarded as the combination of the typical bimodal one and its rotated components. For specimens annealed at higher temperatures (500 °C and 550 °C), the ring-like basal texture remains the main characteristic even without considerable change in textural intensity (Figures 9(e) and (f)). Note that for all the specimens with the ring-like basal texture, the recrystallization either proceeds to a significant extent (Figures 6(d) and (e)) or is already completed (Figure 6(f)), which must be responsible for such textural evolution.

Figure 10 presents a further analysis of deviation angles (φ) between *c*-axis and the ND for all the specimens. For the as-rolled specimen, Figure 10(a) shows that its φ prefers to concentrate on 20 to 40 and 90 deg, which agrees with the bimodal basal textural component and the c//TD component revealed in Figure 9(a). As expected, the distribution of φ in the 350 °C-annealed specimen is almost identical with that of the as-rolled specimen (Figure 10(b)). After annealing at higher temperatures, although the recrystallization begins to occur and produce evident textural variation, the φ seems to maintain its preferable distribution between 20 and 40 deg (Figures 10(c) through (f)). Nevertheless, the frequency of φ near 90 deg is always reduced with increasing temperature, as a result of the recrystallization.

C. Hardness Variation

Figure 11 shows the hardness variation of the as-rolled HP-Ti sheet during annealing at 350 °C to 450 °C. The as-rolled specimen has an average hardness value of 234.3 ± 5.8 HV. After annealing at 350 °C for 1 hours, although recrystallization is not initiated at all, the average hardness drops to 215.2 ± 5.4 HV. With increasing the annealing temperature, the specimen hardness decreases continuously with the lowest one (135.9 ± 2.9 HV) obtained for the fully recrystallized specimen (550 °C-annealed). In the following, in-depth reasons accounting for the hardness evolution will be analyzed and discussed in terms of the above illustrated microstructural and textural characteristics to quantitatively clarify main controlling factors.

IV. DISCUSSION

A. Microstructural and Textural Evolution

In earlier studies,^[11,23,26,27] it has been widely reported that the bimodal basal texture (occasionally denoted as $\{11\bar{2}5\}\langle 10\bar{1}0 \rangle$) developed in heavily rolled α -Ti sheets was rather stable during annealing and would be well maintained even after complete primary recrystallization. For example, Wagner *et al.*^[26] figured out that the typical deformation texture of a 80 pct cold-rolled CP-Ti sheet was essentially unchanged after annealing at 500 °C for 6 hours, even if primary recrystallization had

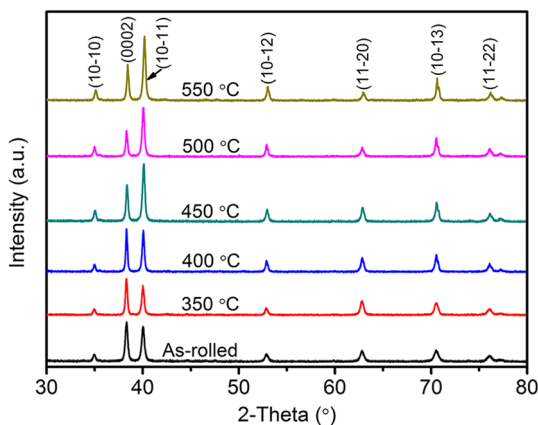


Fig. 8—XRD patterns of various specimens.

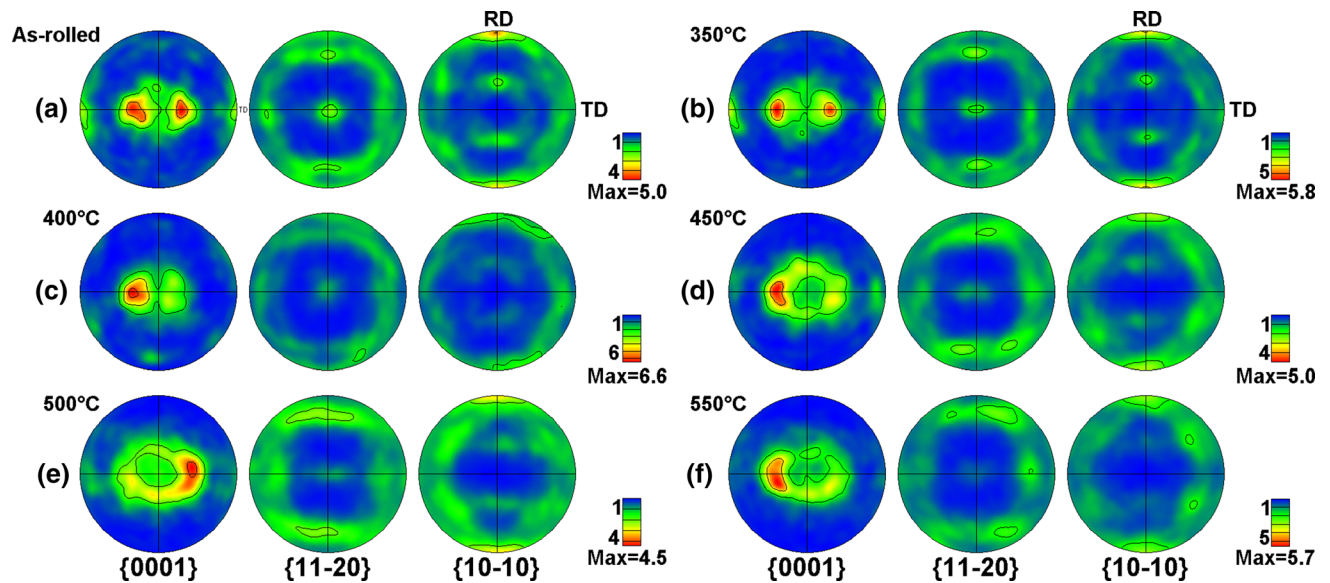


Fig. 9—Pole figures of the (a) as-rolled HP-Ti sheet and specimens annealed at various temperatures: (b) 350 °C, (c) 400 °C, (d) 450 °C, (e) 500 °C, and (f) 550 °C, respectively, with each one corresponding to an EBSD scanning area of $1000 \times 800 \mu\text{m}^2$ (step size of 10 μm).

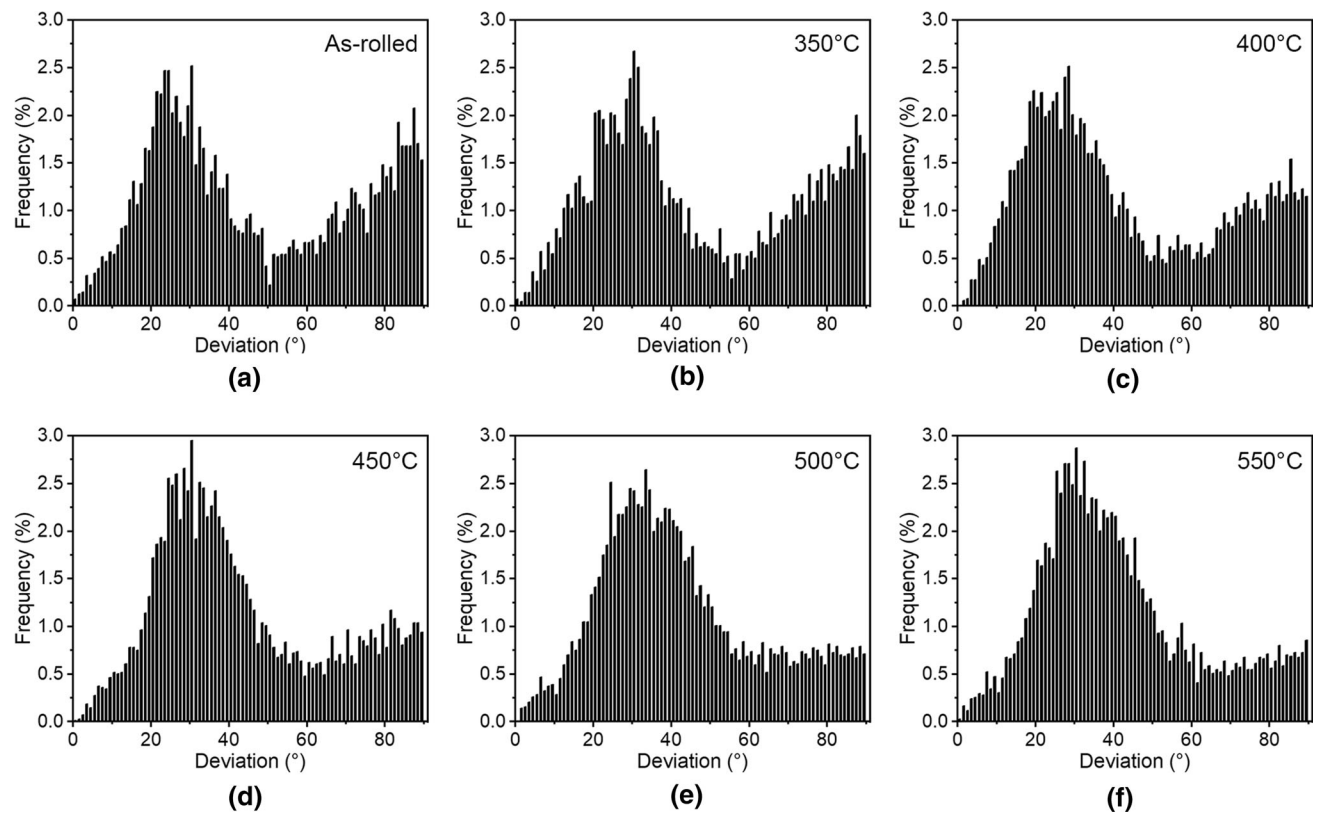


Fig. 10—Deviation angles between c -axis and ND in the (a) as-rolled HP-Ti sheet and specimens annealed at various temperatures: (b) 350 °C, (c) 400 °C, (d) 450 °C, (e) 500 °C, and (f) 550 °C, respectively, derived from the same EBSD data as in Fig. 9.

been finished (with fully equiaxed grains). Only after extensive annealing to allow sufficient grain growth (like at 700 °C for 1 hours), grain orientations could gradually develop to form the so-called “recrystallization texture” ($\{10\bar{1}3\}\langle 11\bar{2}0\rangle$), which anyhow still showed bimodal maxima in the basal pole figure.

Clearly, such a usual scenario is different from our finding in the present work. Through Figures 1 through 10, we demonstrate that both microstructural and textural characteristics of the 50 pct cold-rolled HP-Ti sheet can change markedly during the primary recrystallization. After 50 pct cold rolling, our HP-Ti sheet develops

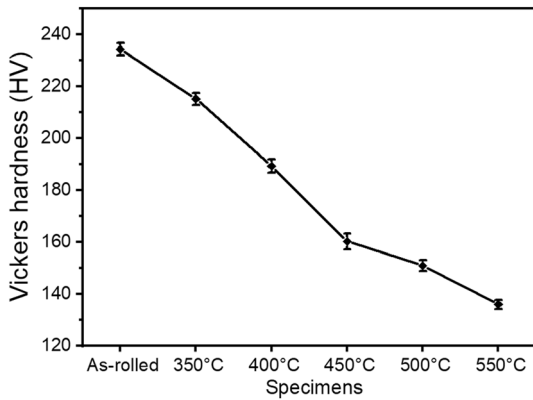


Fig. 11—Evolution of Vickers hardness of the as-rolled HP-Ti sheet and specimens annealed at various temperatures.

a typical deformation texture ($\{11\bar{2}5\}\langle 10\bar{1}0\rangle$), as shown in Figure 9(a). However, main features of such texture are maintained only after annealing at 400 °C or lower temperatures so that recrystallization nucleation is still in the early stage (Figures 9(b) and (c)). At higher temperatures (like 450 °C and 500 °C), even if 1-hour-annealing does not allow the recrystallization to be completed, a ring-like basal texture with evident differences from the deformation texture can be developed (Figures 9(d) and (e)). For the 550 °C-annealed specimen with fully recrystallized structures, the ring-like basal texture is still present suggesting considerable stability (Figure 9(f)). To our best knowledge, such a textural evolution feature of rolled pure Ti sheets during annealing has not been reported in public literature.

To better understand the role played by recrystallization in changing textural characteristics during annealing, the 400 °C- and the 450 °C-annealed specimens (both with partly recrystallized structures) are selected for further analyses. They are subjected to large-area EBSD scanning so that deformed and recrystallized structures including enough orientations can be obtained, with results presented in Figures 12 and 13.

Figure 12(a) is the large-area BC map of the 400 °C-annealed specimen, from which recrystallization nuclei are found to preferably appear near prior grain boundaries. During the prior 50 pct rolling, the HP-Ti sheet consisting of coarse equiaxed grains are heavily deformed jointly by continuous slip and twinning, as demonstrated through Figures 1(a) through 5(a). In the meantime, prior grain boundaries will strongly impede dislocation movement and twinning growth, leading to larger plastic strains and misorientations often accumulated in such locations.^[28,29] As a result, recrystallization nucleation will prefer to happen near these boundaries. Figures 12(b) and (c) are IPF maps of the deformed and the recrystallized structures extracted from Figure 12(a), with their pole figures displayed in Figures 12(d) and (e), respectively. Clearly, those unrecrystallized structures have the strong bimodal basal texture while more scattered orientations are obtained for the recrystallization nuclei. Since the area fraction of the unrecrystallized structures (~80.2 pct) is much higher than that of

(~19.8 pct) the recrystallized structures in Figure 12, the 400 °C-annealed specimen still shows main features of the typical deformation texture (Figure 9(c)).

A similar analysis is made for the 450 °C-annealed specimen with a higher fraction (~74.6 pct) of recrystallized structures, as presented in Figure 13. For the unrecrystallized structures (Figure 13(d)), they still have the same bimodal basal texture as that of the as-rolled specimen (Figure 9(a)). For the recrystallized structures, a ring-like textural feature with the reduced *c*//TD component can be noticed in the basal pole figure (Figure 13(e)), clearly different from the deformation texture.

Through Figures 12 and 13, one can confirm that orientations of recrystallization nuclei/grains do not simply maintain those in the as-rolled Ti sheet, in not agreement with earlier reports.^[11,12,26] Note that since primary recrystallization is still uncompleted in our 400 °C- and the 450 °C-annealed specimens, such textural variation should not be ascribed to sufficient grain growth as noted in References 23, 26. Thus, new orientations must have been generated during the recrystallization nucleation to give birth to the textural features shown in Figures 12(e) and 13(e). Two main nucleation mechanisms have been reported for α -Ti alloys during recrystallization annealing^[30]: (i) strain-induced boundary migration (SIBM) and (ii) orientation-gradient-related subgrain coalescence. The SIBM mechanism involves the bulging of parts of a preexisting HAB with different stored energies on two sides and is featured by new grains having similar orientations to the old ones, inconsistent with our results. As for the second mechanism, when there exists a large orientation gradient (often along with high stored energy induced by geometrically necessary dislocations), HABs can be produced by subgrain growth/coalescence *via* rapid recovery. As a result, new recrystallization nuclei with orientations different from any preexisting ones are generated, then allowing distinct textural components to be produced. In an earlier study, Bozzolo *et al.*^[31] found that large orientation gradients could be produced near HABs in heavily rolled CP-Ti owing to strong interaction between dislocations and boundaries. Compared to CP-Ti, denser HABs can be introduced into the rolled HP-Ti sheet by more active twinning due to the absence of impurities, as verified in our recent work.^[8] Furthermore, relatively large orientation gradients are indeed found to readily exist inside grains in the 50 pct -rolled HP-Ti specimen, as clearly exemplified in Figure 14. Based on the above analysis, it is reasonable to expect that the orientation-gradient-related subgrain coalescence mechanism has played an important role in the recrystallization nucleation process, eventually giving birth to the new textural feature in the annealed HP-Ti specimens (Figures 9(d) through (f)). Nevertheless, along with new orientations, the global textures of recrystallized structures (Figures 12(e) and 13(e)) are found to always contain the bimodal basal component (deformation texture), suggesting the SIBM may have also worked to some extent.

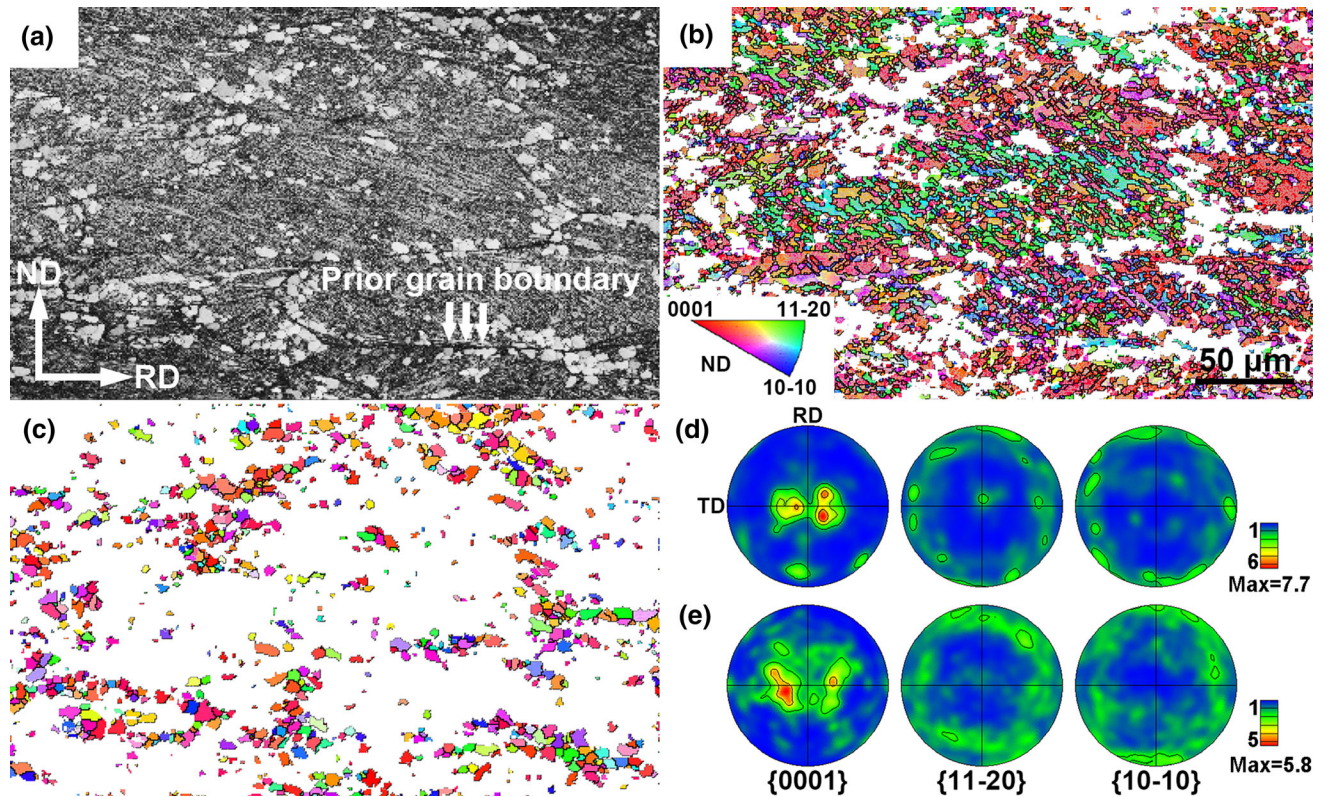


Fig. 12—Dedicated EBSD analysis (scanning area of $330 \times 200 \mu\text{m}^2$ and step size of $0.8 \mu\text{m}$) for the $400 \text{ }^\circ\text{C}$ specimen: (a) BC map; (b) and (c) IPF maps of deformed and recrystallized structures extracted from (a), respectively; (d) and (e) pole figures corresponding to (b) and (c), respectively.

B. Correlation Between Microstructure, Texture, and Hardness

The hardness of the as-rolled HP-Ti sheet is found to decrease continuously with increasing annealing temperatures. Its high purity (> 99.99 wt pct) suggests there will be essentially no compositional variation during annealing and the hardness change could thus be mainly ascribed to two factors: grain size (determined based on HABs) and dislocation content (mainly stored in LABs). Their specific contributions could be analyzed quantitatively by the use of the EBSD statistical data of microstructural parameters. For the HP-Ti sheet, its overall strength $\sigma_{0.2}$ (0.2 pct proof stress) can be expressed as,^[32,33]

$$\sigma_{0.2} = \sigma_0 + \sigma_{LAB} + \sigma_{HAB}, \quad [1]$$

where σ_0 is the lattice friction stress of α -Ti (~ 290 MPa^[7]), and σ_{LAB} and σ_{HAB} are the strengthening contributions from LABs and HABs, respectively. The σ_{LAB} can be further expressed as,^[34]

$$\sigma_{LAB} = M\alpha Gb\sqrt{\rho_0 + \rho_{LAB}}, \quad [2]$$

where M is the Taylor factor (3.0 for α -Ti^[35]), α is a constant (0.2), G is the shear modulus (43.6 GPa^[7]), b is the Burgers vector (0.347 nm ^[35]), ρ_0 is the dislocation density between boundaries in a sufficiently annealed material and often negligible due to being

too small, and ρ_{LAB} is the density of dislocations stored in LABs that can be expressed by Reference 33.

$$\rho_{LAB} = \frac{3\bar{\theta}_{LAB}(1 - f_{HAB})}{bD_{av}}, \quad [3]$$

where $\bar{\theta}_{LAB}$ is the average misorientation angle of LABs in each specimen, f_{HAB} is the fraction of HABs and D_{av} is the average spacing between all boundaries. The above parameters can be calculated by the HKL channel 5 software from EBSD data and tabulated in Table I.

The contribution from HABs follows the Hall–Petch law but can be re-expressed in another equivalent form^[36]:

$$\sigma_{HAB} = k_{HP}\sqrt{\frac{f_{HAB}}{D_{av}}}, \quad [4]$$

where k_{HP} is the Hall–Petch slope with a typical value of $240 \text{ MPa } \mu\text{m}^{1/2}$ for α -Ti.^[37]

After inputting the structural parameters in Table I into Eqs. [2], [3], and [4], σ_{LAB} and σ_{HAB} can be obtained for each specimen, as tabulated in Table II. The calculated results in Table II agree with the measured hardness of each specimen, verifying the validity of the above quantitative analysis. Generally, Table I and II reveal that with increasing annealing temperature, the fraction of HABs increases at the expense of LABs, leading to reduced strengthening/hardening

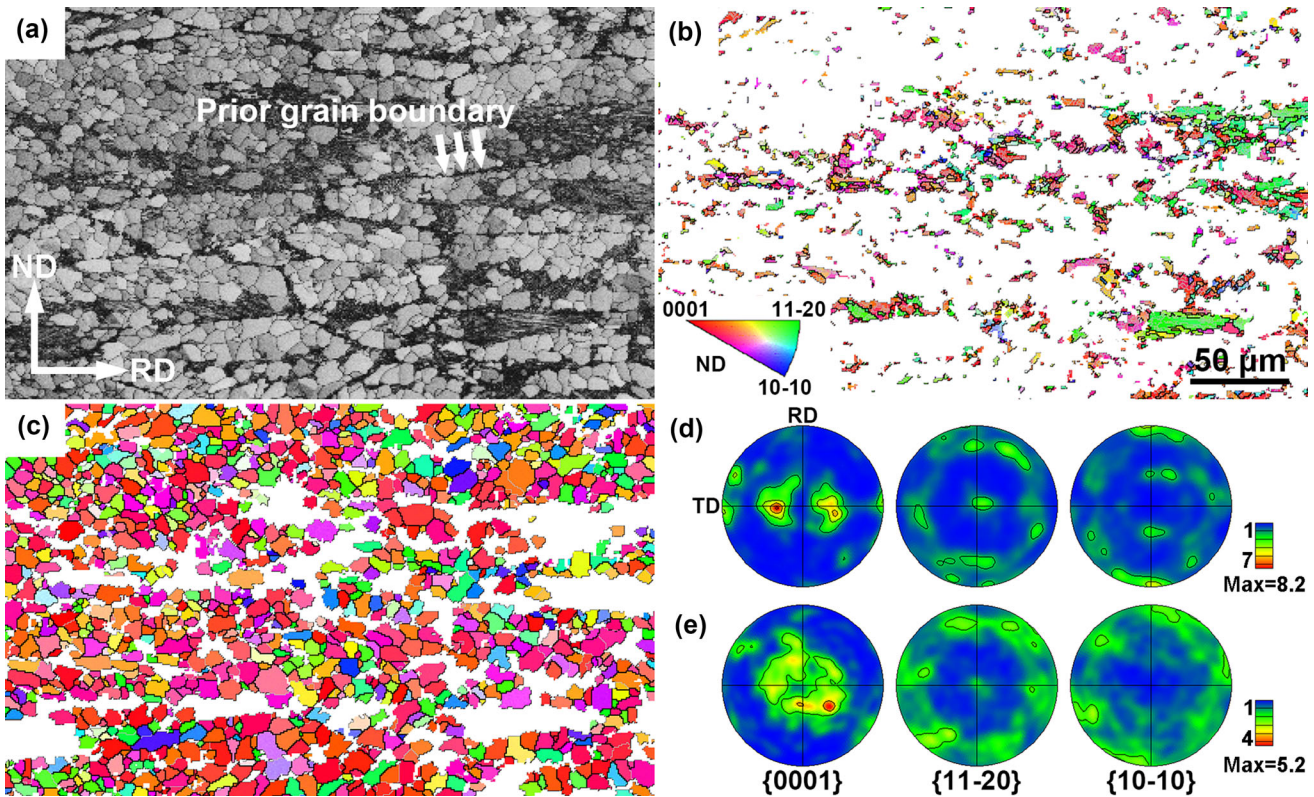


Fig. 13—Dedicated EBSD analysis (scanning area of $330 \times 200 \mu\text{m}^2$ and step size of $0.8 \mu\text{m}$) for the $450 \text{ }^\circ\text{C}$ specimen: (a) BC map; (b) and (c) IPF maps of deformed and recrystallized structures extracted from (a), respectively; (d) and (e) pole figures corresponding to (b) and (c), respectively.

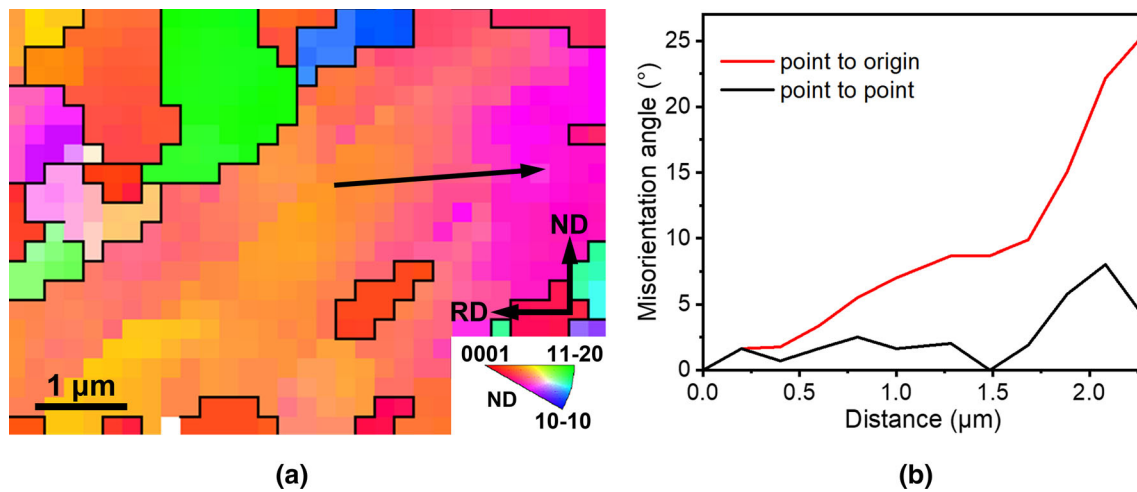


Fig. 14—(a) IPF map of a selected location in the 50 pct-rolled specimen and (b) misorientation variations along the arrowed path in (a), demonstrating the presence of large orientation gradients inside grains.

contributions from both of them. Specifically, when the annealing temperature increases from $400 \text{ }^\circ\text{C}$ to $450 \text{ }^\circ\text{C}$, both the σ_{LAB} and the σ_{HAB} are found to drop drastically (almost halved), in contrast with mild change at lower temperatures. According to the above results, significant recrystallization has occurred in the $450 \text{ }^\circ\text{C}$ -annealed specimen, which should be responsible for such drastic change. After annealing at higher

temperatures, the change of σ_{HAB} becomes relatively mild again while the σ_{LAB} further decreases. This suggests that releasing stored energy *via* eliminating LABs is able to soften the HP-Ti sheet more effectively than increasing grain sizes during annealing.

In spite of overall consistency, one may note that there are still some deviations between the measured and the calculated hardnesses in Table II. One reason might

Table I. Structural Parameters of Various Specimens Measured by EBSD

Structural Parameters	Specimens					
	As-Rolled	350 °C	400 °C	450 °C	500 °C	550 °C
f_{HAB} (Pct)	49.1	52.0	54.1	63.1	72.5	90.3
f_{LAB} (Pct)	50.9	48.0	45.9	36.9	27.5	9.7
$\bar{\theta}_{\text{LAB}}$ (rad $\times 10^{-2}$)	8.4	8.6	8.6	8.9	10.8	16.9
D_{av} (μm)	0.9	1.1	1.1	4.7	5.6	5.7

Table II. Calculated and Measured Hardnesses of Various Specimens

Strength/hardness	Specimens					
	As-Rolled	350 °C	400 °C	450 °C	500 °C	550 °C
σ_{LAB} (MPa)	184.3	163.9	159.7	70.7	61.3	45.2
σ_{HAB} (MPa)	177.3	165.0	168.3	87.9	86.4	95.5
$\sigma_{0.2}$ (MPa)	651.6	618.9	618.0	448.6	437.7	430.7
Calculated Hardness (HV) ^a	217.2	206.3	206.0	149.5	145.9	143.6
Measured Hardness (HV)	234.3	215.2	189.3	160.2	150.9	135.9

^aCalculated using a well-accepted empirical expression, $3 \text{ HV} \approx \sigma_{0.2}$.

be some inaccuracy caused by empirical parameters and experimental errors during collecting and post-processing the EBSD data. In addition, recent work^[38,39] demonstrated that angles between grain *c*-axes and the loading axis would definitely affect hardness of α -Ti. When its *c*-axis was perpendicular to the loading direction (deviation angle $\varphi = 90$ deg), the grain had the lowest hardness, which increased gradually with reducing φ . In the present work, the loading direction during hardness measurements is parallel to the ND of all the specimens. This allows the relationship between grain orientations and hardness to be analyzed using results in Figure 10. Figure 10(a) through (c) reveals that the φ of the as-rolled specimen and the specimens annealed at 350 °C and 400 °C preferably concentrates on ~ 30 and ~ 90 deg. After annealing at higher temperatures (450 °C to 550 °C), the φ peak near 30 deg is almost unchanged while the grains with $\varphi = \sim 90$ deg are largely reduced (Figures 10(d) through (f)). This indicates that one major change occurring during annealing at higher temperatures is the reduced fraction of soft-orientation grains (φ near 90 deg). This may be able to produce additional hardening. However, since the specimen hardness is found to decrease continuously with raising annealing temperatures, such an additional hardening effect is expected to be relatively weak.

V. CONCLUSIONS

- (1) For the 50 pct-rolled HP-Ti sheet, recrystallization nucleation starts at 400 °C with prior grain boundaries as preferential sites while fully

- recrystallized structures were obtained after annealing at 550 °C for 1 hours
- (2) Considerable textural changes occur during recrystallization annealing of the as-rolled HP-Ti sheet, namely, the prior bimodal basal texture characteristic is essentially replaced by a ring-like basal texture, which can be attributed to the orientation-gradient-related subgrain coalescence mechanism.
- (3) Hardness changes during annealing are found to be closely related to grain sizes and dislocation densities (mainly stored in low-angle boundaries). Quantitative analyses reveal that effects of both of them are relatively mild after annealing below 450 °C. However, the decrease in dislocation density would lead to more significant softening than grain coarsening when the annealing temperature exceeds 450 °C.

ACKNOWLEDGMENTS

This work was financially supported by the Postdoctoral Science Foundation of China (2021M690174), the Graduate Student Innovation Program of Chongqing University of Technology (CLGYCX20202003), the Open Foundation of Guangxi Key Laboratory of Processing for Non-ferrous Metals and Featured Materials at Guangxi University (2021GXYSOF06), the National Natural Science Foundation of China (52171052 and 51901193), and the Sichuan Science and Technology Program (2020ZDZX0017-3).

CONFLICT OF INTEREST

The authors declare that they have no conflict of interest.

REFERENCES

1. D. Banerjee and J.C. Williams: *Acta Mater.*, 2013, vol. 61, pp. 844–79.
2. J. Dai, J. Xia, L. Chai, K.L. Murty, N. Guo, and M.R. Daymond: *J. Mater. Sci.*, 2020, vol. 55, pp. 8346–62.
3. J.M. Cordeiro and V.A.R. Barao: *Mater. Sci. Eng. C.*, 2017, vol. 71, pp. 1201–15.
4. M.-S. Lee, M.-K. Ji, Y.-T. Hyun, E.-Y. Kim, and T.-S. Jun: *Mater. Charact.*, 2021, vol. 172, p. 110834.
5. S. Zhao, R. Zhang, Q. Yu, J. Ell, R.O. Ritchie, and A.M. Minor: *Science.*, 2021, vol. 373, pp. 1363–68.
6. A. Ghosh: *Int. J. Fatigue.*, 2019, vol. 120, pp. 12–22.
7. S.V. Zherebtsov, G.S. Dyakonov, A.A. Salem, V.I. Sokolenko, G.A. Salishchev, and S.L. Semiatin: *Acta Mater.*, 2013, vol. 61, pp. 1167–78.
8. J. Dai, L. Zeng, Z. Li, L. Chai, Z. Zheng, H. Wu, K.L. Murty, and N. Guo: *Sci. China Technol. Sci.*, 2019, vol. 62, pp. 1968–75.
9. A.O.F. Hayama and H.R.Z. Sandim: *Mater. Sci. Eng. A.*, 2006, vol. 418, pp. 182–92.
10. S.-W. Choi, C.-L. Li, J.W. Won, J.-T. Yeom, Y.S. Choi, and J.-K. Hong: *Mater. Sci. Eng. A.*, 2019, vol. 764, p. 138211.
11. A. Ghosh, A. Singh, and N.P. Gurao: *Mater. Charact.*, 2017, vol. 125, pp. 83–93.
12. S.K. Sahoo, S. Panda, R.K. Sabat, G. Kumar, S.C. Mishra, U.K. Mohanty, and S. Suwas: *Philos. Mag.*, 2015, vol. 95, pp. 1105–24.
13. C.K. Yan, A.H. Feng, S.J. Qu, G.J. Cao, J.L. Sun, J. Shen, and D.L. Chen: *Acta Mater.*, 2018, vol. 154, pp. 311–24.
14. M.L. Wasz, F.R. Brotzen, R.B. McLellan, and A.J. Griffin: *Int. Mater. Rev.*, 2013, vol. 41, pp. 1–12.
15. Q. Yu, L. Qi, T. Tsuru, R. Traylor, D. Rugg, J.W. Morris Jr., M. Asta, D.C. Chrzan, and A.M. Minor: *Science.*, 2015, vol. 347, pp. 635–39.
16. H. Conrad: *Prog. Mater. Sci.*, 1981, vol. 26, pp. 123–403.
17. C. Ouchi, H. Iizumi, and S. Mitao: *Mater. Sci. Eng. A.*, 1998, vol. 243, pp. 186–95.
18. A. Issariyapat, P. Visuttipitukul, J. Umeda, and K. Kondoh: *Addit. Manuf.*, 2020, vol. 36, p. 101537.
19. N. Liu, Y. Wang, W.-J. He, J. Li, A. Chapuis, B.-F. Luan, and Q. Liu: *T. Nonferr. Met. Soc. China.*, 2018, vol. 28, pp. 1123–31.
20. F.J. Humphreys: *J. Mater. Sci.*, 2001, vol. 36, pp. 3833–54.
21. N. Bozzolo, L. Chan, and A.D. Rollett: *J. Appl. Crystallogr.*, 2010, vol. 43, pp. 596–602.
22. S. Xu, M. Gong, Y. Jiang, C. Schuman, J.-S. Lecomte, and J. Wang: *Acta Mater.*, 2018, vol. 152, pp. 58–76.
23. N. Bozzolo, N. Dewobroto, T. Grosdidier, and F. Wagner: *Mater. Sci. Eng. A.*, 2005, vol. 397, pp. 346–55.
24. J.W. Won, T. Lee, S.-G. Hong, Y. Lee, J.H. Lee, and C.S. Lee: *Met. Mater. Int.*, 2016, vol. 22, pp. 1041–48.
25. S.I. Wright, M.M. Nowell, and D.P. Field: *Microsc. Microanal.*, 2011, vol. 17, pp. 316–29.
26. F. Wagner, N. Bozzolo, O. Van Landuyt, and T. Grosdidier: *Acta Mater.*, 2002, vol. 50, pp. 1245–59.
27. H.-T. Jiang, J.-X. Liu, Z.-L. Mi, A.-M. Zhao, and Y.-J. Bi: *Int. J. Min. Met. Mater.*, 2012, vol. 19, pp. 530–35.
28. G.S. Dyakonov, S. Mironov, S.V. Zherebtsov, S.P. Malysheva, G.A. Salishchev, A.A. Salem, and S.L. Semiatin: *Mater. Sci. Eng. A.*, 2014, vol. 607, pp. 145–54.
29. G. Salishchev, S. Mironov, S. Zherebtsov, and A. Belyakov: *Mater. Charact.*, 2010, vol. 61, pp. 732–39.
30. Y.B. Chun, S.L. Semiatin, and S.K. Hwang: *Acta Mater.*, 2006, vol. 54, pp. 3673–89.
31. N. Bozzolo, N. Dewobroto, H.R. Wenk, and F. Wagner: *J. Mater. Sci.*, 2007, vol. 42, pp. 2405–16.
32. N. Hansen: *Scripta Mater.*, 2004, vol. 51, pp. 801–06.
33. L. Chai, B. Luan, D. Xiao, M. Zhang, K.L. Murty, and Q. Liu: *Mater. Des.*, 2015, vol. 85, pp. 296–308.
34. D.A. Hughes and N. Hansen: *Acta Mater.*, 2000, vol. 48, pp. 2985–3004.
35. P. Luo, D.T. McDonald, W. Xu, S. Palanisamy, M.S. Dargusch, and K. Xia: *Scripta Mater.*, 2012, vol. 66, pp. 785–88.
36. X. Zhang, N. Hansen, Y. Gao, and X. Huang: *Acta Mater.*, 2012, vol. 60, pp. 5933–43.
37. A. Ghaderi and M.R. Barnett: *Acta Mater.*, 2011, vol. 59, pp. 7824–39.
38. Y. Xu, S. Joseph, P. Karamched, K. Fox, D. Rugg, F.P.E. Dunne, and D. Dye: *Nat. Commun.*, 2020, vol. 11, p. 5868.
39. A. Fitzner, J. Palmer, B. Gardner, M. Thomas, M. Preuss, and J.Q. da Fonseca: *J. Mater. Sci.*, 2019, vol. 54, pp. 7961–74.

Publisher's Note Springer Nature remains neutral with regard to jurisdictional claims in published maps and institutional affiliations.